Etch-tuning and Design of SiN Photonic Crystal Reflectors

Simon Bernard,[1] Christoph Reinhardt,[1] Vincent Dumont,[1] Yves-Alain Peter,[2] Jack C. Sankey[1]

[1] *Department of Physics, McGill University, Montréal, Québec, H3A 2T8, Canada*
[2] *Department of Engineering Physics, Polytechnique, Montréal, Québec, H3C 3A7, Canada*
simon.bernard@mail.mcgill.ca

Abstract: We tune a freestanding photonic crystal reflector resonance to within 0.15 nm (0.04 linewidths) of 1550 nm using iterative hydrofluoric acid etches, and provide design considerations for creating reflectors robust against beam collimation.

OCIS codes: 230.5298, 220.4241, 230.4040

By etching a 2D photonic crystal into a freestanding dielectric membrane, it is possible to resonantly enhance the membrane's normal-incidence reflectivity at a specific wavelength [1]. Such photonic crystal reflectors (PCRs) are attractive for the field of optomechanics [2], wherein the reduced mass and increased reflectivity both serve to increase light's influence over the membrane's motion. However, standard nanolithography techniques cannot reliably produce crystals with the resonance at a pre-specified wavelength, to match (e.g.) that of a low-noise laser, an atomic transition, or another crystal. To overcome this limitation (for Si_3N_4, at least), we fabricate a crystal initially having too much material, and then perform a series of hydrofluoric (HF) acid dips to iteratively tune its resonance to a convenient (telecom) wavelength $\lambda_0 = 1550$ nm. We also perform a series of simulations for these structures, and discuss design considerations for realizing high-reflectivity in the presence of a Gaussian collimated beam. More details can be found in Ref. [3].

Our PCRs are fabricated from a Si wafer coated with stoichiometric Si_3N_4. Membranes are initially released with a combination of backside photolithography, a reactive ion etch (RIE; removes nitride), and a KOH wet-etch (removes silicon). The crystal is then patterned into the membrane using electron-beam lithography and RIE, and the whole structure is then thinned with HF. Figure 1(a)-(c) show the 66-nm-thick PCR as fabricated, and Fig. 1(d), curve (i) shows how its transmission $\mathcal{T}$ depends on wavelength λ for a 60-μm-diameter Gaussian beam (red dot in Fig. 1(a)). The crystal resonance appears as a minimum $\mathcal{T}_{\min}$ at $\lambda_r = 1566$ nm. We then iteratively dip this crystal in HF and measure $\mathcal{T}(\lambda)$ (Fig. 1(d), curves (ii)-(iv)); by the third iteration (curve (iv)), the resonant wavelength resides within 0.15 nm (0.04 linewidths) of our target $\lambda_0 = 1550$ nm. Simulations (grey curves) predict an integrated thickness change of 8 nm, consistent with a reflectometer measurement of 9 ± 1 nm. The rate of λ_r is found to fluctuate somewhat between iterations (-4.4 nm/min (i $\rightarrow$ ii), -3.2 nm/min (ii $\rightarrow$ iii), and -7.9 nm/min (iii $\rightarrow$ iv)), which can be mitigated by introducing fluid flow during the etch and/or by using a less aggressive HF solution and shorter dips.

Consistent with literature [4,5], the plane-wave simulations (of an infinite crystal with periodic boundary conditions [6]) in Fig. 1(d) predict a transmission dip that is both deeper and narrower than is observed for these thin Si_3N_4 crystals. As discussed elsewhere [3,7], the observed resonance broadening likely arises from the superposition of plane waves – each having a different incidence angle θ ($\theta = 0$ corresponds to normal incidence) – present in a Gaussian collimated beam, and the resonant wavelength's dependence on θ. To see this, note that, near a minimum in $\mathcal{T}$, the transmission can be approximated $\mathcal{T} \approx \frac{1}{2}(\partial_\lambda^2 \mathcal{T})(\lambda - \lambda_r)^2$. Additionally, keeping only the leading-order θ-dependence, the resonant wavelength $\lambda_r \approx \frac{1}{2}(\partial_\theta^2 \lambda_r)\theta^2$ (assumed by symmetry and verified by simulation). We can therefore average this approximate form of $\mathcal{T}(\lambda)$ over all incidence angles θ, weighted by the collimated beam's Gaussian distribution ($\propto e^{-2\theta^2/\theta_D^2}$ for $\theta_D \ll 180°$; in our case, $\theta_D = 1°$, as drawn in Fig. 1(d)'s inset), which produces an overall transmission minimum that is shifted by $\Delta\lambda_r \approx \frac{1}{8}\left(\partial_\theta^2 \lambda_r\right)\theta_D^2$ and (more importantly) raised to a value $\mathcal{T}_{\min} \approx \frac{1}{192}(\partial_\theta^4 \mathcal{T})\theta_D^4$. A useful figure of merit is therefore the prefactor $\frac{1}{192}\partial_\theta^4 \mathcal{T}$, which provides a relative comparison of collimation-induced broadening for different crystal geometries, and a quick estimate of $\mathcal{T}_{\min}$ (provided $\mathcal{T}_{\min} \ll 1$).

Figure 1(e) shows a map of many simulated crystal geometries achieving $\lambda_r = \lambda_0$ for a variety of hole diameter d, lattice constant a, and thickness h (all scaled by λ_0), and Fig. 1(f) shows this figure of merit for each. These results illustrate that the thickest simulated crystals (specifically near $a = 0.77\lambda_0$) should be the most robust against collimation broadening. In the context of optomechanics, this implies a potential compromise between attainable reflectivity and mechanical mass.

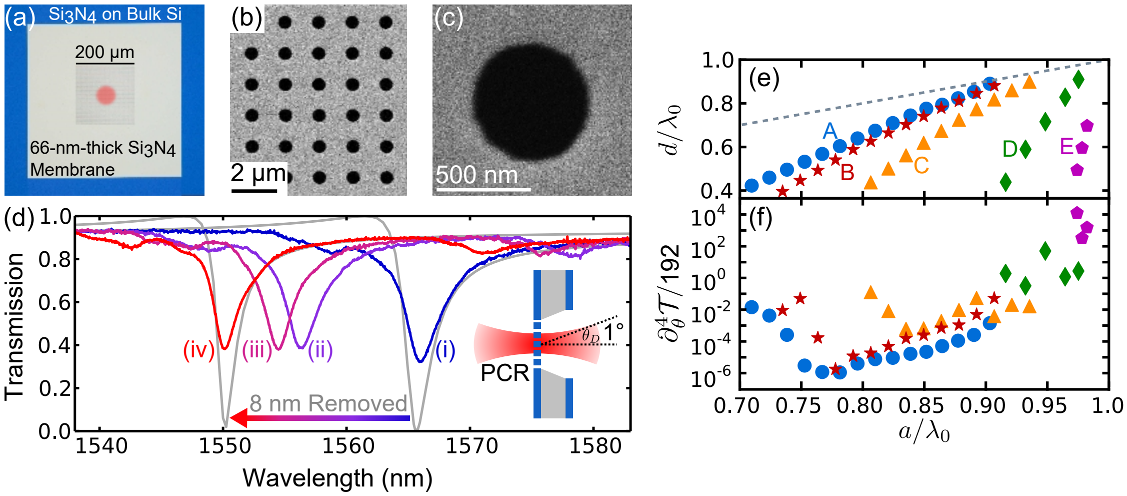

Fig. 1. (a) Freestanding Si_3N_4 PCR. The red spot indicates the $1/e^2$ laser diameter with divergence angle $\theta_D \sim 1°$ drawn in (d). (b) Crystal with hole diameter d=614 nm (±7 nm hole-to-hole with edge roughness ∼15 nm) and lattice constant a=1500 ± 6 nm. (c) Zoom-in. (d) Transmission spectrum for the crystal as fabricated (i) and then iteratively immersed in HF acid for (ii) 130 s, and (iii) 165 s and (iv) 195 s (total), reducing h by 9 ± 1 nm and increasing d by ∼4 nm. Grey curves show the simulated response to normal-incidence plane waves, assuming refractive index 2, hole diameters (i) 614 nm and (iv) 618 nm and thicknesses (i) 62.5 nm and (iv) 54.5 nm. (e) Parameter space of Si_3N_4 PCRs with (a,d) combinations producing a resonant wavelength λ_r within 0.3% of the targeted λ_0 for h=0.26λ_0 (circles), h=0.19λ_0 (stars), h=0.13λ_0 (triangles), h=0.065λ_0 (diamonds), and h=0.032λ_0 (pentagons). Dashed line indicates the geometrical limit $d = a$. (f) Figure of merit. A-E denote "optimal" (a,d) combinations (of those simulated).

References

1. W. Zhou, D. Zhao, Y.-C. Shuai, H. Yang, S. Chuwongin, A. Chadha, J.-H. Seo,K. X. Wang, V. Liu, Z. Ma, and S. Fan, "Progress in 2D photonic crystal Fano resonance photonics," Progress in Quant. Electron. **38**, 1 (2014).
2. M. Aspelmeyer, T. J. Kippenberg, and F. Marquardt, "Cavity optomechanics," Rev. Mod. Phys. **86**, 1391 (2014).
3. S. Bernard, C. Reinhardt, V. Dumont, Y.-A. Peter, and J. C. Sankey, "Precision resonance tuning and design of SiN photonic crystal reflectors," Opt. Lett. **41**, 5624-5627 (2016).
4. C. H. Bui, J. Zheng, S. W. Hoch, L. Y. T. Lee, J. G. E. Harris, and C. Wei Wong, "High-reflectivity, high-Q micromechanical membranes via guided resonances for enhanced optomechanical coupling," Appl. Phys. Lett. **100**, 21110 (2012).
5. R. A. Norte, J. P. Moura, and S. Groblacher, "Mechanical Resonators for Quantum Optomechanics Experiments at Room Temperature," Phys. Rev. Lett. **116**, 147202 (2016).
6. A. F. Oskooi, D. Roundy, M. Ibanescu, P. Bermel, J. D. Joannopoulos, and S. G. Johnson, "Meep: A flexible free-software package for electromagnetic simulations by the FDTD method," Comput. Phys. Commun. **181**, 687 (2010).
7. K. B. Crozier, V. Lousse, O. Kilic, S. Kim, S. Fan, and O. Solgaard, "Air-bridged photonic crystal slabs at visible and near-infrared wavelengths," Phys. Rev. B **73**, 115126+ (2006).